Applied Catalysis B: Environmental 147 (2014) 642–650

Contents lists available at ScienceDirect

Applied Catalysis B: Environmental

journal homepage: www.elsevier.com/locate/apcatb

Visible light photocatalytic activities of nitrogen and platinum-doped TiO_2: Synergistic effects of co-dopants

Wooyul Kim[a], Takashi Tachikawa[b], Hwajin Kim[a], Narayanan Lakshminarasimhan[a,c], Palanichamy Murugan[c], Hyunwoong Park[d], Tetsuro Majima[b], Wonyong Choi[a,*]

[a] School of Environmental Science and Engineering, Pohang University of Science and Technology (POSTECH), Pohang 790-784, Republic of Korea
[b] The Institute of Scientific and Industrial Research (SANKEN), Osaka University, Mihogaoka 8-1, Ibaraki, Osaka 567-0047, Japan
[c] CSIR–Central Electrochemical Research Institute (CECRI), Karaikudi 630 006, Tamil Nadu, India
[d] School of Energy Engineering, Kyungpook National University, Daegu 702-701, Republic of Korea

ARTICLE INFO

Article history:
Received 26 June 2013
Received in revised form 5 September 2013
Accepted 22 September 2013
Available online 29 September 2013

Keywords:
Visible light photocatalysis
Titanium dioxide
Dopants
Band structure
Photooxidation and photoreduction

ABSTRACT

The visible light photocatalytic activity of nitrogen doped TiO_2 (N-TiO_2) was enhanced with co-doping of Pt ions for the oxidative and reductive degradation of model substrates in gaseous and aqueous phases. The synthesized samples were characterized by various techniques (diffuse reflectance UV–Vis, XPS, XRD, FT-IR, HR-TEM, EDX and laser flash photolysis spectroscopy). The co-doping of N and Pt of TiO_2 (Pt,N-TiO_2) significantly enhanced the degradation of acetaldehyde (gas phase), and trichloroacetate (TCA) (aqueous phase), and the reduction of Cr(VI) (aqueous phase) under visible light ($\lambda > 420$ nm). The observed visible light photocatalytic activity of Pt,N-TiO_2 was markedly higher than the singly-doped TiO_2 (Pt-TiO_2 or N-TiO_2). A time-resolved diffuse reflectance (TDR) study found that the presence of the different oxidation states of Pt (2+ and 4+) plays a crucial role in the charge trapping and transfer dynamics in Pt-TiO_2. The TDR study of Pt,N-TiO_2 further revealed that the synergistic effect of co-doping is attributed to the combined contribution of each dopant. Finally, the first principle calculations for the doped TiO_2 suggested that the electronic interaction of Pt and N in TiO_2 facilitates the charge carrier mobility and reduces the undesired recombination, leading to enhanced photocatalytic activity.

1. Introduction

TiO_2 is the most extensively studied photocatalyst owing to high photoactivity, low cost, non-toxicity, and high stability [1–4]. The absence of visible light activity resulting from wide bandgap (3.0–3.2 eV), however, limits its widespread application. A variety of approaches have been attempted to make TiO_2 function under visible light [5–8]. Among them, doping with metals [9–11] and non-metals [12–14] into TiO_2 lattice has been widely employed to reduce the bandgap energy by creating new energy levels between the conduction and valence bands [15,16]. Although single element-doped TiO_2 can usually absorb visible light, unfortunately, the visible light photocatalytic activity is low as compared to its UV light induced activity. Such low visible light activity results primarily from an enhanced recombination of electron–hole pairs at the dopant-created defect sites and the lower redox potentials of the electron and hole generated under visible light.

As an alternative approach, doping with two or more elements (co-doping) has been explored in order to improve the photocatalytic activity and stability of single element-doped TiO_2 [17]. Among them, metal and non-metal elements (mostly N) are often co-doped such as Pd–N [18], Fe–N [19,20], W–N [21], and Mo–N [22]. However, co-doped TiO_2 does not always display better photocatalytic activity than that of the single element-doped TiO_2 and even the enhanced activity is found only for some specific reactions [11]. Such inconsistent behavior and limited activities of co-doped TiO_2 imply that the roles of dopants are complex. To address this issue, the roles of dopants and the related dynamics of photogenerated charge carriers in the photocatalysis of co-doped TiO_2 should be understood. However, there are few studies on this.

With this in mind, this study investigated the simultaneous doping effect of Pt and N on TiO_2-photocatalysis for the conversion of gaseous acetaldehyde and aqueous trichloroacetate (TCA) under visible light ($\lambda > 420$ nm). The photocatalytic reduction of hexavalent chromium (Cr(VI) → Cr(III)) was also carried out to estimate the reduction ability of photogenerated electron under visible light. A recent study shows that the nitridation of Pt-TiO_2 enhanced the visible light photocatalytic activity yet such enhancement depends on the Pt electronic state and the nature of substrate [23]. The co-doping of Pt ion can improve the photocatalytic activity of N-TiO_2 with the formation of combined Pt and N induced mid-gap levels. This may contribute synergistically to efficient hole transfer. If so, the charge carrier dynamics will be different between the bare and doped samples. In this regard, a time-resolved diffuse reflectance

* Corresponding author. Tel.: +82 54 279 2283.
E-mail address: wchoi@postech.edu (W. Choi).

0926-3373/$ – see front matter © 2013 Elsevier B.V. All rights reserved.
http://dx.doi.org/10.1016/j.apcatb.2013.09.034

(TDR) spectroscopic study was performed to understand the generation, relaxation, recombination and interfacial charge transfer of photogenerated electrons and holes with the bare and doped TiO_2 samples. Finally, an attempt has been made to correlate the photocatalytic activities with the observed transient dynamics and theoretical density of states (DOS) calculations.

2. Experimental

2.1. Synthesis of materials

Doped TiO_2 powder was prepared with a wet chemical method. The chemicals used includes titanium tetraisopropoxide (TTIP, $Ti(OCH(CH_3)_2)_4$, Aldrich), ethanol (Aldrich), chloroplatinic acid (H_2PtCl_6, Aldrich), ammonium hydroxide (NH_4OH, Aldrich), and nitric acid (HNO_3, Shinyo). For nitrogen-doped TiO_2 (N-TiO_2), a mixed solution of TTIP (1.25 mL) and ethanol (25 mL) was added dropwise to distilled water (250 mL) adjusted to pH 1.5 with nitric acid. In this solution, 10 mL of aqueous ammonia (28% solution) was added at 0 °C with stirring and the resulting gel was filtered, washed with water, dried, and calcined. For calcination, as-synthesized TiO_2 powder was gradually heated in air at a rate of 1 °C/min to 400 °C and kept at this temperature for 3 h. Then the calcined TiO_2 powder was washed to remove the impurities (e.g., chlorides and nitrates) and dried. For platinum-doped TiO_2 (Pt-TiO_2), the aforementioned TTIP and ethanol mixture solution was added dropwise to 250 mL of chloroplatinic acid solution at pH 1.5. The typical Pt concentration was 0.08 mM, corresponding to 0.5 atom% with respect to Ti at which the highest visible light activity was obtained [10]. The resulting sol was stirred overnight and evaporated at 60 °C using a rota-vapor. The obtained powder was annealed in air following the aforementioned calcination procedure. Bare TiO_2 powder was prepared by following the same synthesis procedure of Pt-TiO_2 in the absence of chloroplatinic acid.

Pt and N co-doped TiO_2 powder (Pt,N-TiO_2) was prepared by combining the above two methods. First, TTIP dissolved in absolute ethanol was dropped into the chloroplatinic acid solution and stirred overnight. Then an aqueous solution (10 mL) of 28% ammonia was added and stirred continuously. The white precipitate was filtered, washed and calcined following the aforementioned procedure.

2.2. Characterization

The phase formation and purity of the synthesized TiO_2 samples were analyzed with a powder X-ray diffraction (XRD) technique with Cu-*K* radiation (Mac Science Co. M18XHF). The surface area was analyzed by the Brunauer–Emmett–Teller (BET) method using a Micromeritics ASAP 2000 instrument (see Fig. S2). Diffuse reflectance UV–Visible (DRUV–Vis) absorption spectra of the powder samples were recorded using a spectrophotometer (Shimadzu UV-2401 PC) with an integrating sphere attachment, and $BaSO_4$ or bare TiO_2 was used as a reference. Fourier transform infrared (FT-IR) spectroscopic technique (ABB Bomem, MB series) was employed to find the presence of nitrogen-containing species and self-supporting thin pellets were used to record the spectrum. The X-ray photoelectron spectroscopic (XPS, Kratos, XSAM 800pci) technique with an Mg *K* source (1253.6 eV) was used to find the electronic states of the elements. The binding energies of all peaks were calibrated against the C 1s line (284.6 eV) originating from the surface impurities. The high-resolution transmission electron micrographs (HR-TEM) and energy-dispersive X-ray (EDX) analysis of doped TiO_2 samples were obtained using a JEM-2100F microscope with Cs-correction.

2.3. Photocatalytic and photoelectrochemical activity tests

For the evaluation of photocatalytic activities, gaseous acetaldehyde, aqueous trichloroacetate, and aqueous Cr(VI) were selected as model compounds because they are well-known pollutants and their degradation/conversion mechanisms are relatively well established [3,4,10,24–26]. The photocatalytic oxidation of acetaldehyde (CH_3CHO) was carried out in a closed-circulation reactor at ambient conditions using acetaldehyde (300 ppmv in N_2) as the standard gas with a carrier gas (Ar (99.9999%), O_2 (99.9999%)) [24]. The typical inlet concentration of acetaldehyde was 60 ppmv. The adsorption test for acetaldehyde indicates the amounts of acetaldehyde adsorbed are 1278, 1237, 1238 and 1252 ppmv (*gas-phase equivalent*) for Pt-, N-, Pt,N-TiO_2 and bare TiO_2, respectively. The photocatalytic activities of the synthesized TiO_2 powders were evaluated in terms of the degradation of trichloroacetate (TCA, CCl_3CO_2Na, Aldrich) and conversion of Cr(VI) ($Na_2Cr_2O_7{\cdot}2H_2O$, Aldrich). The detailed experimental procedure is provided in Appendix A.

2.4. Time-resolved diffuse reflectance (TDR) measurements

The TDR spectroscopy measurements were performed using the third harmonic generation (355 nm, 5 ns full width at half-maximum) and the second harmonic generation (532 nm, 2.0 mJ/pulse, 5 ns fwhm) from a Q-switched Nd^{3+}:YAG laser (Continuum, Surelite II-10) [27–29]. The reflected analyzing light from a pulsed 450-W Xe arc lamp (Ushio, UXL-451-0) was collected by a focusing lens and directed through a grating monochromator (Nikon, G250) to a silicon avalanche photodiode detector (Hamamatsu Photonics, S5343). The transient signals were recorded by a digitizer (Tektronix, TDS 580D). The reported signals are averages of 30–100 events. Sample suspensions were saturated with oxygen gas before irradiation to make the photocatalytic reaction reversible. All experiments were performed at room temperature.

2.5. Computational methodology

To understand the electronic properties of Pt-, N- and Pt,N-TiO_2, the first principles calculations were performed within the frame work of the density functional theory using the Vienna Ab-initio Simulation Package (VASP). Atoms were described by a plane wave-based projector augmented wave (PAW) formalism [30] and the exchange interaction between the electrons was corrected by generalized gradient approximations (GGA). The kinetic cut-off energy for a plane wave of 400 eV was also used. The supercell is constructed with a $2 \times 2 \times 1$ unit-cell and it contains 16 Ti and 32 O atoms. To mimic the Pt-TiO_2 system, Pt atom was substituted at Ti site, while for Pt,N-TiO_2, N atom was introduced either at interstitial site or at oxygen site. The optimized lattice constants ($a = b = 3.776$ Å, and $c = 9.486$ Å) were used for performing entire calculations. The Briullouin zone (BZ) of the supercell was sampled with a $4 \times 4 \times 4$k-mesh. All atoms were repeatedly relaxed by conjugate gradient approximations, until the force of ions attains a value below ± 0.01 eV/Å. To obtain the electronic density of the states, non-self consistence calculations were carried out with Gaussian broadening of 0.1 eV.

3. Results and discussion

3.1. Electronic states of dopants

The phase formation and purity of the synthesized bare, Pt-, N-, and Pt,N-TiO_2 samples were examined by powder X-ray diffraction (XRD). The XRD patterns show that all samples are of single phase with an anatase structure (Fig. S1). It is noted that N-TiO_2 has

higher crystallinity than other samples, which can be ascribed to the different preparation conditions: bare, Pt-, and Pt,N-TiO_2 were prepared in acidic condition (in the presence of nitric acid and/or chloroplatinic acid) whereas N-TiO_2 was synthesized in basic condition (in the presence of ammonium hydroxide). A basic condition appears to favor the formation of anatase. For example, Huang et al. reported that the presence of NH_3 in the synthesis of N-TiO_2 led to the higher crystallinity [31]. The BET surface areas of bare, N-, Pt-, and Pt,N-TiO_2 were measured to be 110, 64, 124, and 178 m^2/g, respectively (see Fig. S2 for more detailed description on the porous nature of samples). The HR-TEM images show that the three doped-TiO_2 samples are all similar in their crystal lattice structure and morphology (Fig. S3). The EDX analysis shows no significant signals for dopants, which indicates that the Pt and N dopants are well dispersed in the TiO_2 lattice, not concentrated in the surface region.

The doping induced the coloration of TiO_2: pale yellow (N-TiO_2), yellowish brown (Pt-TiO_2) and brownish yellow (Pt,N-TiO_2) (Fig. S4). The diffuse reflectance UV–Visible (DRUV–Vis) absorption spectra of bare and doped TiO_2 samples are shown in Fig. 1. Doped TiO_2 samples exhibit similar main absorption edges with bare TiO_2, indicating that the band gap of the host TiO_2 is not altered. However, the dopants increase the absorption in the visible region with the greatest degree for Pt-TiO_2. To clearly identify the visible light absorption portion, the spectra of N-, Pt- and Pt,N-TiO_2 were recorded using the bare TiO_2 as a reference instead of $BaSO_4$ (Fig. 1 inset). In Pt-TiO_2, the main absorption is observed at 420 nm with a distinct shoulder at ca. 560 nm. The visible absorption of Pt-TiO_2 may be attributed to the electronic transitions between the Pt redox states and the band edge of TiO_2 [10]. A previous study found that both Pt^{2+} and Pt^{4+} could exist in Pt-TiO_2 since the surface Pt atoms are coordinatively unsaturated [10]. Under this circumstance, the intervalence charge transfer between Pt^{2+} and Pt^{4+} is allowed and results in the visible absorption at ~560 nm, which is similar to the one observed in Pt complexes [32]. This absorption shoulder at ~560 nm is absent in Pt,N-TiO_2, which may imply that the electronic states of Pt in Pt,N-TiO_2 are different from those of Pt-TiO_2. Such a difference is possible since the synthetic conditions adopted for Pt-TiO_2 and Pt,N-TiO_2 were different. The former was synthesized by acid hydrolysis of TTIP whereas the synthesis of the latter was performed in basic condition in the presence of NH_4OH as the nitrogen precursor. Pt is employed in the form of H_2PtCl_6 in situ during the TiO_2 synthesis. It is known that $PtCl_6^{2-}$ exists as varying species ($PtCl_{6-x}(OH)_x$) depending on pH during hydrolysis [33]. The synthesis at different pH may lead to the different electronic states of Pt between Pt-TiO_2 and Pt,N-TiO_2.

The absorption spectra clearly show that the band edge of N-TiO_2 is not shifted. N-doping only increases the light absorption in the region between 400 and 550 nm leaving the band edge of TiO_2 unaltered. A similar effect of N-doping in metal oxides was reported [34]. It was theoretically shown that the π and π^* molecular orbitals formed by NO species lie just below and above the valence band (VB) of TiO_2, respectively, when N occupies the interstitial site in the lattice [12,35]. Our result consistently shows that N-doping leads to the creation of interstitial N 2p states lying above the VB of TiO_2, while the true band gap narrowing is not observed (e.g., see Fig. 10 and discussion). The true narrowing of the original band gap of the metal oxide semiconductor needs heavy doping of anion or cation; yet such condition results in different stability of the phase from that of anatase TiO_2 [36]. The FT-IR spectroscopic technique was used to monitor the N species in TiO_2 since N can be incorporated as an interstitial species forming NO_x species in TiO_2 lattice. It is found that N-TiO_2 has an absorption band at 1637 cm^{-1} (Fig. S5). Similarly, Pt,N-TiO_2 also shows a weak and broad absorption in the same region. This absorption can be indexed as the stretching vibration of NO group as observed with HONO [37]. Furthermore, this absorption is similar to the bridging bidentate nitrate species as reported in the case of NO_x adsorbed on Al_2O_3 [38]. The FT-IR spectrum of N-TiO_2 further reveals less resolved and weak absorption peaks at 1430 and 1354 cm^{-1} (Fig. S5). These absorption bands are attributed to vibrations of Ti–N bond and surface bound NO_3^- group, respectively [39]. Accordingly, N dopants seem to occupy the interstitial position primarily as NO_x in the TiO_2 lattice.

To examine the electronic states of the dopants, XPS studies were further carried out for Pt and N (Fig. 2). The Pt 4f level exhibits

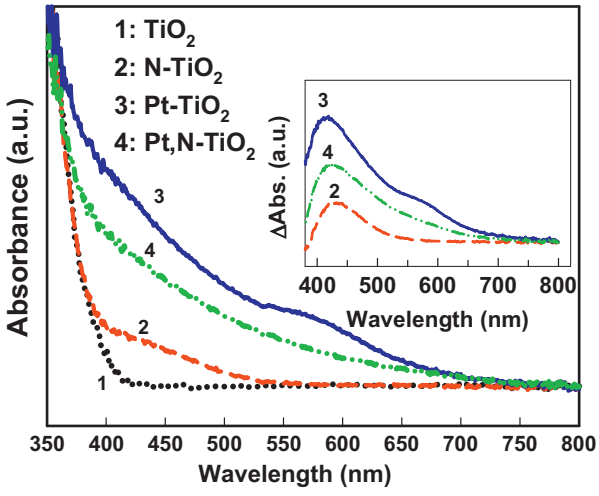

Fig. 1. Diffuse reflectance UV–visible spectra of bare, N-, Pt- and Pt,N-doped TiO_2 ($BaSO_4$ as reference). The insets shows the absorption spectra of N-, Pt-, and Pt,N-TiO_2 recorded with respect to bare TiO_2.

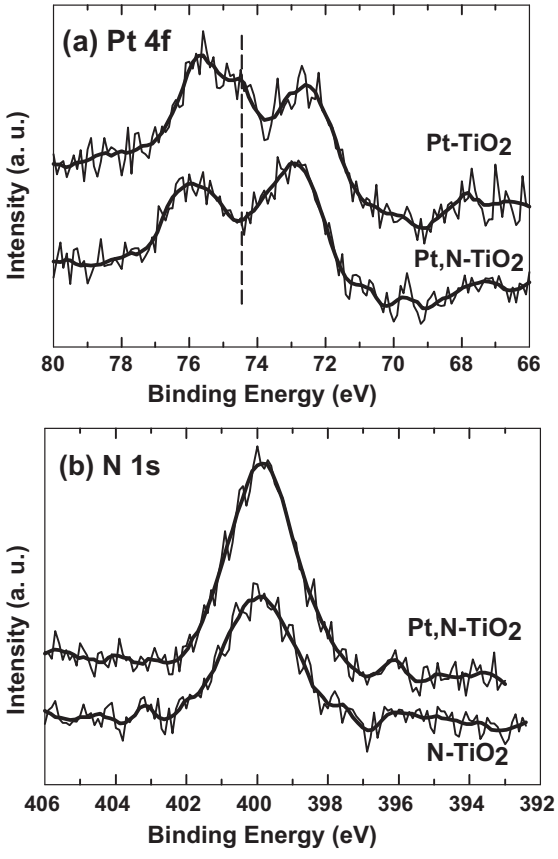

Fig. 2. XPS spectra of (a) Pt 4f and (b) N 1s levels in Pt-, N- and Pt,N-TiO_2.

two peaks corresponding to $4f_{5/2}$ (~76 eV) and $4f_{7/2}$ (~72.5 eV) (Fig. 2a). Both peaks are found at slightly higher binding energies in Pt,N-TiO_2 than those in Pt-TiO_2, revealing the different lattice environment for Pt ions. The observed Pt $4f_{5/2}$ band of Pt-TiO_2 is broader than that of Pt,N-TiO_2 along with an additional peak at ~74.5 eV (indicated by a dotted line in Fig. 2a). This indicates that there is an additional Pt species in Pt-TiO_2, which is assigned to Pt^{2+} coordinated to oxygen atom ($Pt^{II}O$) with binding energies of 72.4 and 74.6 eV for $4f_{7/2}$ level [40]. In the presence of Pt^{2+}, intervalence charge transfer between Pt^{2+} and Pt^{4+} could occur, creating an absorption band at ~560 nm (Fig. 1) [10]. The N 1s spectra of both N-TiO_2 and Pt,N-TiO_2 are also shown at 400 eV (Fig. 2b). When nitrogen is doped as an anion (e.g., as in the case of Ti-N), an N 1s peak is found at 396 eV [12]. Being doped in the form of—Ti–N–O [39], however, a different N 1s peak was found at 401.6 eV. The observed N 1s peak at 400 eV in this study, therefore, indicates that nitrogen is doped primarily as a cationic species (e.g., as a form of–NO_x), which further supports the FT-IR results (Fig. S5).

3.2. Visible light photocatalytic activities

The photocatalytic activities of bare and doped TiO_2 samples were tested for the degradation of acetaldehyde in the gas phase under visible light ($\lambda > 420$ nm) (Fig. 3a). It is obvious that Pt,N-TiO_2 is the most active while Pt- and N-TiO_2 have similar activity in the time-dependent CO_2 evolution from the acetaldehyde degradation. Conversion percentages of the acetaldehyde to CO_2 ($=100\% \times 0.5 \times [CO_2]_{50\,min}/[CH_3CHO]_{ads}$) are estimated to be 0.32%, 2.9%, and 2.7% for bare, N-, and Pt-TiO_2, respectively (see Appendix A for the acetaldehyde adsorption). Simultaneous doping of Pt and N markedly enhances the conversion to 4.3% (>50% increase), which is a clear evidence of the synergistic effect (Table 1). The stability/reusability of Pt-, N- and Pt,N-TiO_2 was also examined with CH_3CHO degradation under visible irradiation (Fig. 3b). The photocatalytic activity is maintained up to three repeated cycles. The slight decrease in the activity in the fourth cycle may be attributed to the surface deactivation by carbonaceous residues accumulated on the catalyst. It seems that the impurity doping in the TiO_2 lattice creates mid-gap levels, which enables the visible light-induced degradation of acetaldehyde. The superiority of Pt,N-TiO_2 for acetaldehyde oxidation can be attributed to the presence of the new impurity doping levels created by the co-doped Pt and N species and/or the change in the charge transfer dynamics and kinetics (Scheme 1).

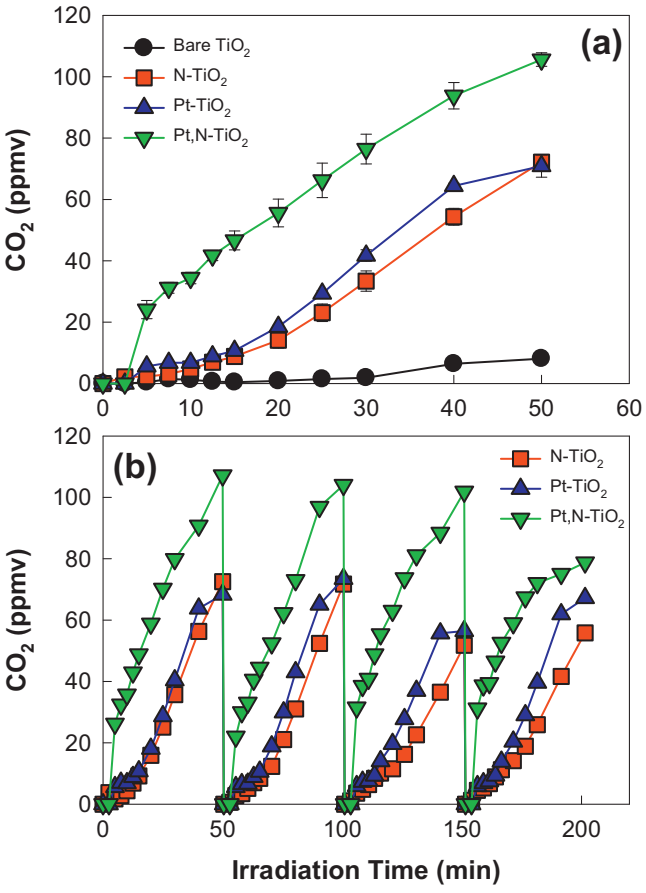

Fig. 3. (a) Time-profiles of CO_2 evolution from the photocatalytic degradation of acetaldehyde pre-adsorbed on bare and doped TiO_2 under visible light ($\lambda > 420$ nm). The amounts of acetaldehyde pre-adsorbed are 1252, 1278, 1237, and 1238 ppmv for bare, Pt-, N-, and Pt,N-TiO_2. (b) Repeated runs for the photocatalytic degradation of acetaldehyde using the same samples (N-, Pt-, and Pt,N-TiO_2).

Table 1
Visible light-induced photocatalytic activities of bare and doped TiO_2 for the degradation of acetaldehyde and trichloroacetate (TCA), and for the reduction of Cr(VI).

	CO_2 from CH_3CHO (ppmv)[a]	Cl^- from TCA (μM)[b]	Cr(VI) (K/min^{-1})[c]
TiO_2 (bare)	8.1	1.9	0.0232
N–TiO_2	72.5	10.2	0.0634
Pt–TiO_2	68.3	27.3	0.0719
Pt,N–TiO_2	107.2	51.0	0.1584

[a] CO_2 generated from the degradation of gaseous CH_3CHO (in 50 min reaction).
[b] Chloride generated from the degradation of TCA in the presence of dissolved O_2 (in 2 h reaction).
[c] The first order rate constant obtained from the removal of Cr(VI).

The photocatalytic activities of bare and doped TiO_2 samples were also tested for the degradation of aqueous trichloroacetate (TCA). In this reaction, the generation of chloride was monitored (Fig. 4a). It has been found that N-TiO_2 has little activity for TCA degradation but Pt- and Pt,N-TiO_2 exhibit higher activities in the following order: Pt,N-TiO_2 > Pt-TiO_2 > N-TiO_2. More important is that the activity of Pt,N-TiO_2 is even greater than the sum of activities of N-TiO_2 and Pt-TiO_2 by 36% (Table 1). The inactivity of N-TiO_2 for TCA suggests either that the initial electron transfer does not occur effectively or that the holes in the mid-gap level created by N-doping are not energetic enough for the oxidation of the dichloroacetate radical intermediate (DRI: $\bullet CCl_2CO_2^-$) under oxic conditions (see Appendix A for detailed discussion on the TCA degradation mechanism) [10,25,41]. Pt-TiO_2 and Pt,N-TiO_2 exhibit higher activities than N-TiO_2 by a factor of 2.7 and 5, respectively. This result further implies that the electrons and holes generated under visible light are energetic enough for the reduction of TCA and the oxidation of the radical intermediates (DRI), respectively [10,25,41]. To demonstrate the reduction ability of the photogenerated electrons under visible irradiation, the photocatalytic reduction of Cr(VI) into Cr(III) was studied as well (Fig. 4b). Both N- and Pt-TiO_2 exhibit similar photocatalytic activities. The observed activity of N-TiO_2 for Cr(VI) reduction indicates that the transfer of photogenerated electron to Cr(VI) is allowed unlike the case of TCA reduction that exhibited little activity with N-TiO_2. This can be attributed to more positive reduction potential of Cr(VI) (+1.36 eV) than that of TCA (−0.49 eV). Pt-TiO_2 exhibits an activity similar to N-TiO_2, whereas Pt,N–TiO_2 exhibits a markedly enhanced activity for the conversion of Cr(VI) (Table 1). This indicates that the photogenerated electrons in Pt,N–TiO_2 are energetic enough to reduce Cr(VI) into Cr(III).

The effective electron transfer on Pt,N-TiO_2 surface was further confirmed by measuring photocurrents collected at a Pt electrode immersed in the catalyst suspension [26,42]. The redox couple of Fe^{3+}/Fe^{2+} was used as an electron shuttle that carries the electron from the TiO_2 to the Pt collector. As compared in Fig. 5, Pt,N–TiO_2

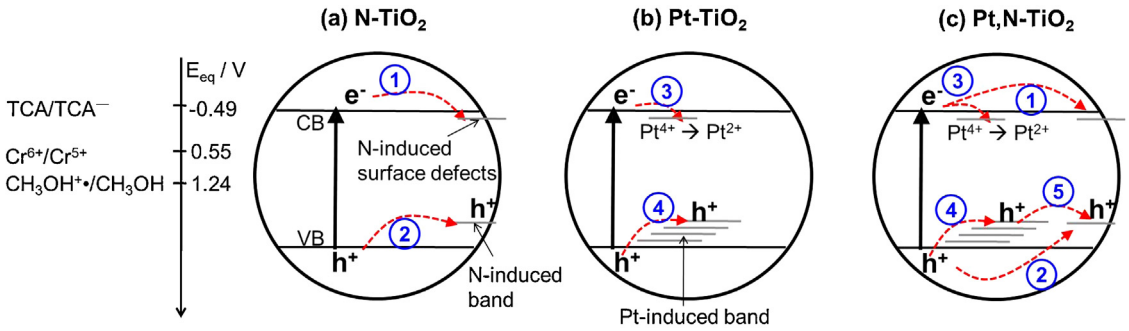

Scheme 1. Schematic illustration for electron and hole trapping in (a) N-TiO_2, (b) Pt-TiO_2, and (c) Pt,N-TiO_2 under 355 nm irradiation. The numbers refer to charge transfer steps: (1) electron trapping on the defect site, (2) hole trapping on the N-induced states, (3) intervalent charge transfer or transition of Pt^{4+} to Pt^{2+}, (4) localization of holes on the Pt-induced band, and (5) hole-hopping. For comparison, the one-electron reduction potentials of the tested substrates are shown on the left side.

generates photocurrent approximately two and three times larger than that of N– and Pt–TiO_2, respectively. This result clearly shows that the photoinduced electron transfer is highly facilitated with the simultaneous doping of N and Pt. This is consistent with the observation that Pt,N–TiO_2 exhibited a markedly enhanced activity for the reductive conversion of both TCA and Cr(VI).

3.3. Charge carrier dynamics

In order to search for the Pt- and/or N-induced surface states, the behaviors of the photogenerated charge carriers in N–, Pt– and Pt,N–TiO_2 samples were analyzed using the time-resolved diffuse reflectance (TDR) spectroscopy during the 355-nm and 532-nm laser photolysis. By monitoring the decay of trapped electron and hole in the absence (i.e., acetonitrile only) and presence of methanol as a hole scavenger, the configuration and roles of the surface states created by single or co-doping can be explored. Fig. 6a shows the observed broad absorption bands of bare TiO_2 in acetonitrile, resulting from the combined effect of trapped holes (ca. 500 nm) and trapped electrons (ca. 700 nm) [27,28,43]. The increase in the absorption band intensity at longer wavelengths in the presence of the hole-scavenging methanol reveals a retarded recombination of the photogenerated electrons in TiO_2 (Fig. 6b). Such behavior (i.e., the retarded recombination of electron by methanol) is more clearly seen in N-TiO_2 (Figs. 6c and d). A higher absorbance at 700 nm for the bare and N-TiO_2 with methanol (Figs. 6b and d, respectively) indicates the higher charge separation yields of the trapped electrons as well as the slower charge recombination kinetics because of the methanol effect [15].

The TDR spectrum of Pt–TiO_2 (Figs. 7a and b) is quite different from those of TiO_2 doped with N, S or C [15,16,28]. Particularly, the trapped electron decay rate at 700 nm is faster than those at other regions (e.g., at 500 nm) in Pt–TiO_2 (Figs. S6c and S7c). The fast electron decay implies a short lifetime of the photogenerated electrons, which might be ascribed to the presence of Pt^{4+} ions acting as electron trapping sites (see reaction S4 in Appendix A). It is of note that Pt-TiO_2 does not show a retarded decay of trapped electrons even in the presence of hole scavenger (methanol) during the 355 nm laser photolysis (Figs. 7b inset). The absence of the

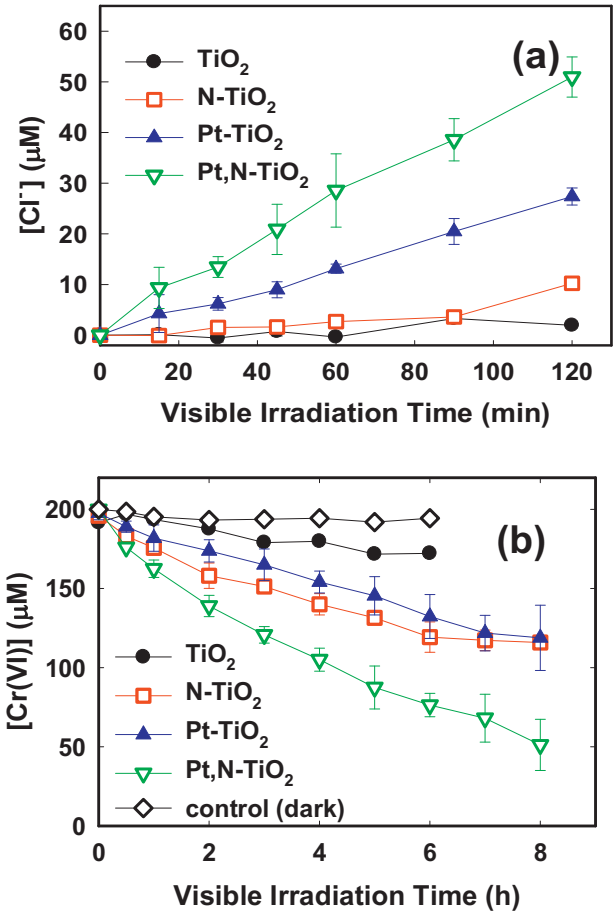

Fig. 4. (a) Time-profiles of chloride generation from trichloroacetate (TCA) degradation and (b) time-profiles of Cr(VI) removal in bare and doped TiO_2 suspensions under visible-light ($\lambda > 420$ nm). $[TCA]_i = 100\ \mu M$; $[Cr(VI)]_i = 100\ \mu M$ (as $Cr_2O_7^{2-}$); [photocatalyst] = 0.5 g/L; pH = 3.0; air-equilibrated.

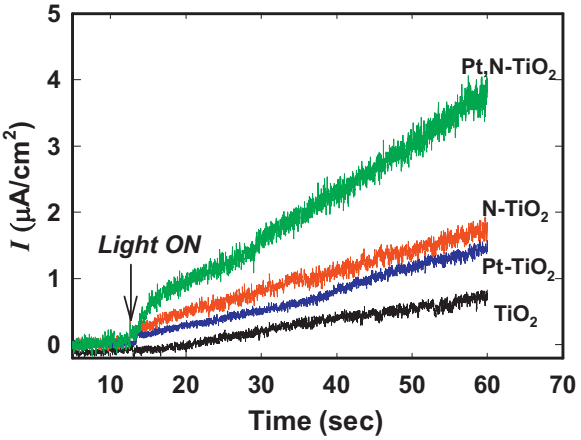

Fig. 5. Time-dependent photocurrent generations in bare and doped TiO_2 suspensions with acetate (electron acceptor) and Fe^{3+} (electron shuttle) under visible light. [photocatalyst] = 0.5 g/L; $[Fe^{3+}] = 0.5$ mM; $[acetate]_0 = 0.2$ M; pH = 2.0; Pt (electron-collecting working electrode) held at +0.4 V; nitrogen-purged continuously.

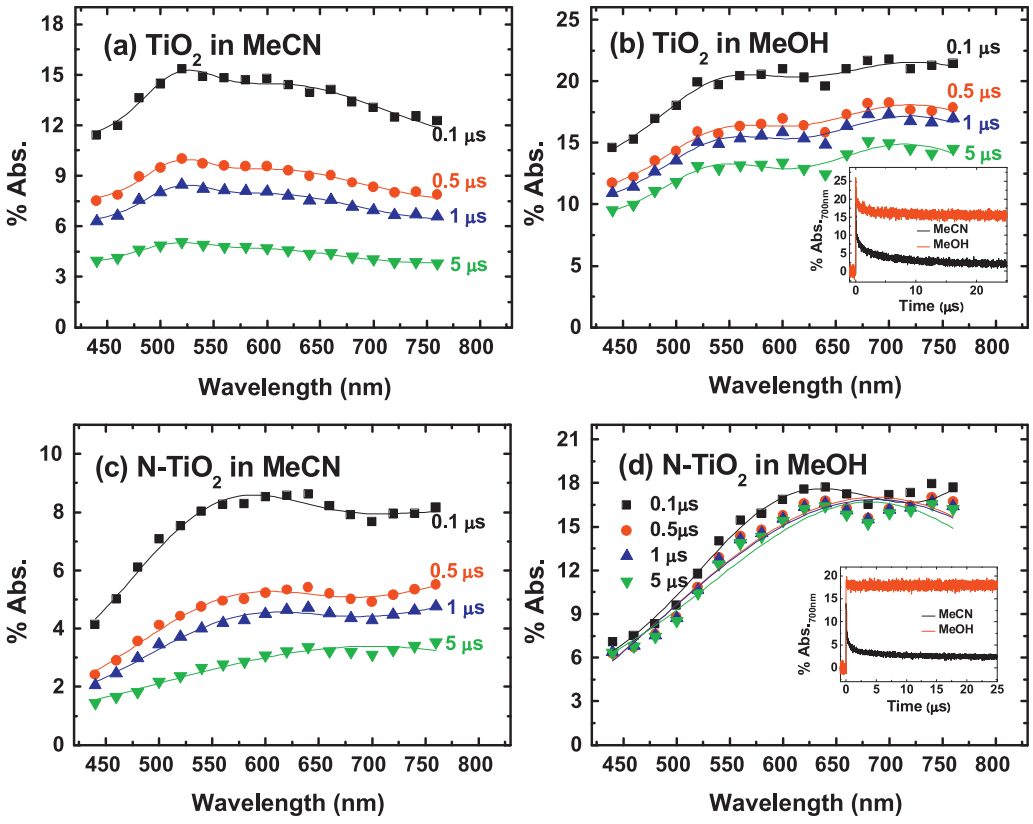

Fig. 6. TDR spectra and time traces observed at 700 nm (inset) during the 355-nm laser photolysis of the TiO_2 (a), (b) and N-TiO_2 (c), (d) in O_2-saturated CH_3CN (a), (c) and CH_3OH (b), (d), respectively.

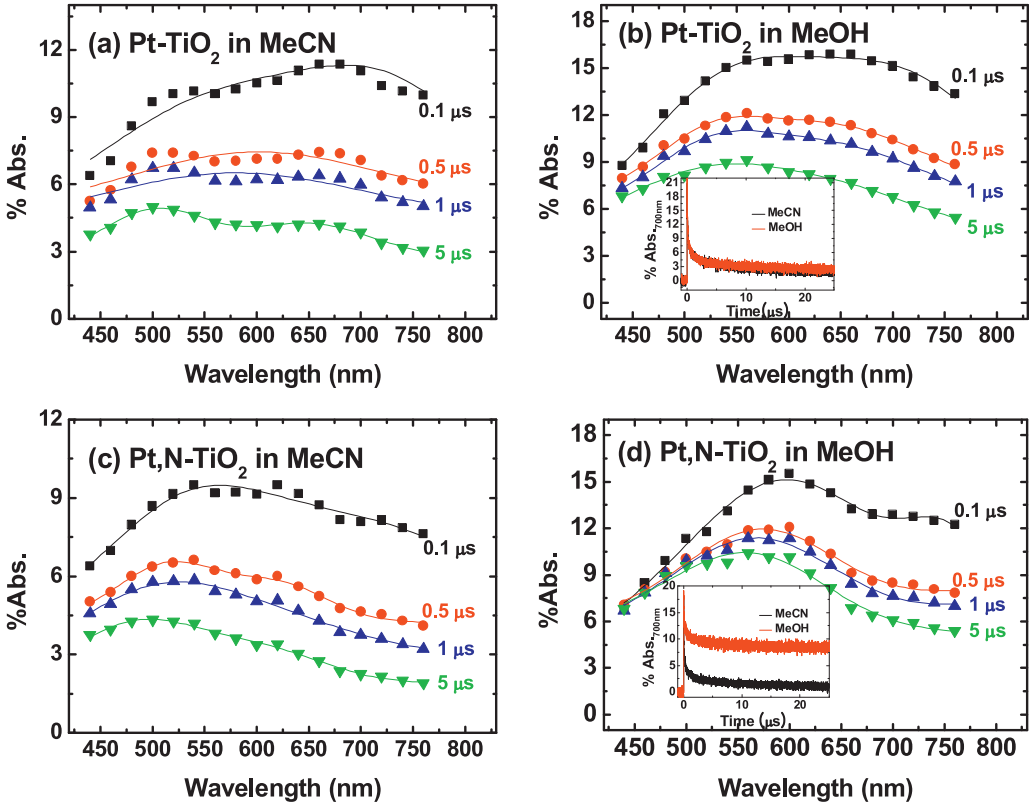

Fig. 7. TDR spectra and time traces observed at 700 nm (inset) during the 355-nm laser photolysis of the Pt–TiO_2 (a), (b) and Pt,N–TiO_2 (c), (d) in O_2-saturated CH_3CN (a), (c) and CH_3OH (b), (d), respectively.

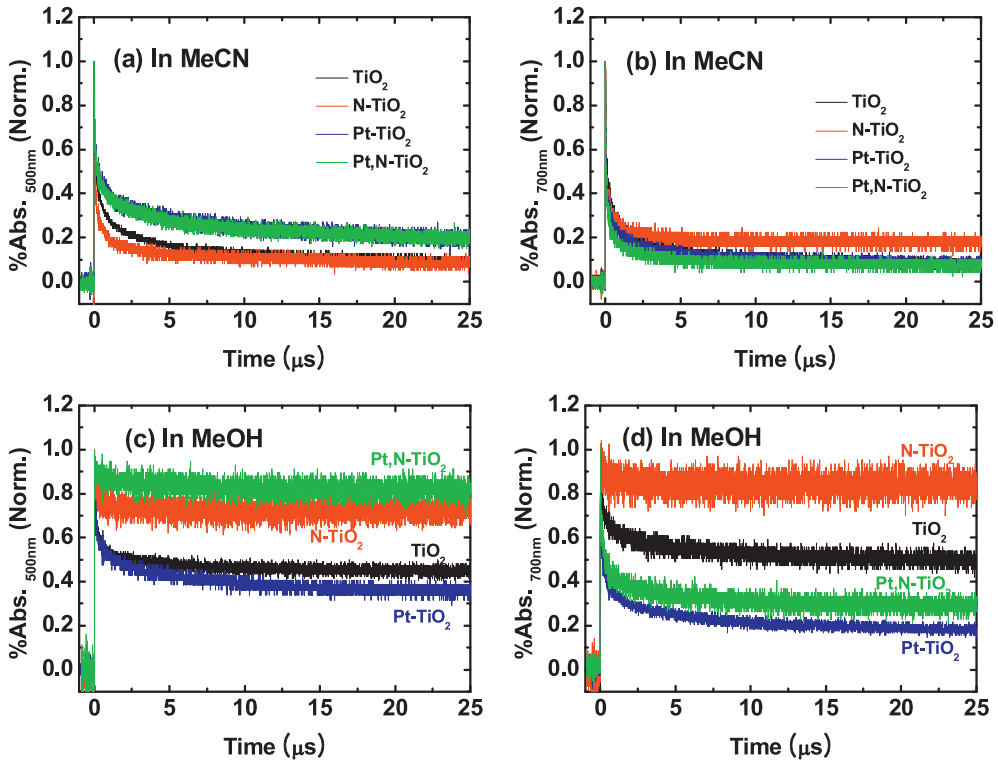

Fig. 8. Normalized time traces observed at 500 nm (a), (c) and 700 nm (b), (d) during the 355-nm laser photolysis of bare, N-, Pt-, and Pt,N-TiO_2 in O_2-saturated CH_3CN (a), (b) and CH_3OH (c), (d), respectively (For interpretation of the references to color in this figure legend, the reader is referred to the web version of this article.).

retarded decay by methanol is clearly distinguished from the cases of TiO_2 and N-TiO_2. This suggests that Pt dopants create energy levels above the valence band edge where the trapped holes are highly localized. The holes trapped (localized) at the midgap states are less energetic and unable to react with methanol (Scheme 1). It is presumed that the partially filled 5d orbitals of Pt^{2+} (d^8) and Pt^{4+} (d^6) modify the electronic structure. The more delocalized Pt 5d orbitals are strongly hybridized with the O 2p orbitals resulting in a wider hybridized valence band. In this situation, the photogenerated holes can be more strongly localized at the hybridized levels in the bulk and are not quenched by methanol on the surface of the catalysts under the 355 nm excitation. The existence of highly localized (i.e., less mobile) holes may lead to a faster charge recombination and consequently the short lifetime of the electron (i.e., absence of methanol effect) during 355 nm laser irradiation. No obvious difference in the electron lifetime either with or without methanol (Fig. 7b inset) confirms this presumption. A similar TDR behavior was also found in iodine-doped TiO_2, wherein the holes are localized and exhibit poor reactivity even under 355 nm excitation [44]. Simultaneous existence of Pt^{2+} and Pt^{4+} in Pt-TiO_2 may lead to the formation of new state by overlapping with the O 2p orbitals.

The TDR spectra of Pt,N-TiO_2 are quite unique and different from N-TiO_2 and Pt-TiO_2 (Figs. 7c and d). The primary difference is the highest retarded time decay of the trapped holes despite the rapid electron decay (see green lines in Figs. 8c and d). This retarded hole quenching by methanol could be attributed to interstate hole hopping from the Pt-induced midgaps to the N-induced surface states. Once hopped into the latter state, the holes may be trapped therein as found in N–TiO_2. Simultaneously, the electron trapping process occurring at the N-induced surface states is inhibited by Pt transition process, resulting in the rapid electron decay (i.e., efficient electron injection to solution). In addition, Pt ion exists exclusively as the Pt^{4+} species in Pt,N-TiO_2 as evidenced by the XPS results and there is no intervalence charge transfer transition (Fig. 1). Due to the absence of the intervalence charge transfer, hole trapping with Pt^{2+} (reaction S5) within the hybridized level is less prominent compared to that of Pt–TiO_2. These electron and hole trappings at the mid-gap levels created by Pt and N dopants are schematically depicted in Scheme 1. These mid-gap levels of different origins in Pt,N-TiO_2 should be responsible for the enhanced charge separation and consequently induce the high photocatalytic activity with a synergistic effect (see Figs. S8–S10 for the 532 nm-laser photolysis).

3.4. Electronic structure of doped TiO_2

It is envisaged that the dopant-created surface states or trap sites should influence the electronic structure of pristine TiO_2. For this, first principles calculations were performed for five possible doping configurations of Pt and N. In the first case, N was introduced at the interstitial site of bulk TiO_2 (N_{int}, Case I). The optimized structure is quite distorted and a –Ti–NO_2–Ti- like species formation has been observed. The calculated Ti–N and N–O bond distances are 2.12 and 1.45 Å, respectively. This result further supports the experimentally observed NO_x species in the FT-IR results (Fig. S5). Our result is also in agreement with an earlier report on the electronic structure of N-doped TiO_2 [35]. For Pt-TiO_2, two different cases were calculated to simulate the system with Pt^{2+} and Pt^{4+} ions as observed experimentally in Pt-TiO_2 (Figs. 1 and 2). To mimic the Pt^{2+} ions in TiO_2 anatase, an oxygen vacancy was created near the Pt site ($Pt^{2+}{}_{Ti}$, Case II), whereas Pt was merely substituted at the Ti site ($Pt^{4+}{}_{Ti}$, Case III) without creating any oxygen vacancy in order to exclusively form the Pt^{4+} ion. In the case of Pt,N-TiO_2, Pt was substituted at the Ti site and N at the interstitial site ($Pt_{Ti} + N_{int}$, Case IV). The optimized structure of Pt,N-TiO_2 is shown in Fig. 9 in which the N atom moves towards one of the O sites, leading to a strong bond with the Pt atom. Subsequently, the N also maintains the interaction with the O and Ti atoms as well. The Ti–N, N–O and Pt–N bond distances are 2.03, 1.32, and 1.91 Å, respectively. This result is different from those of N-TiO_2 in which N occupies the interstitial site and does not move towards

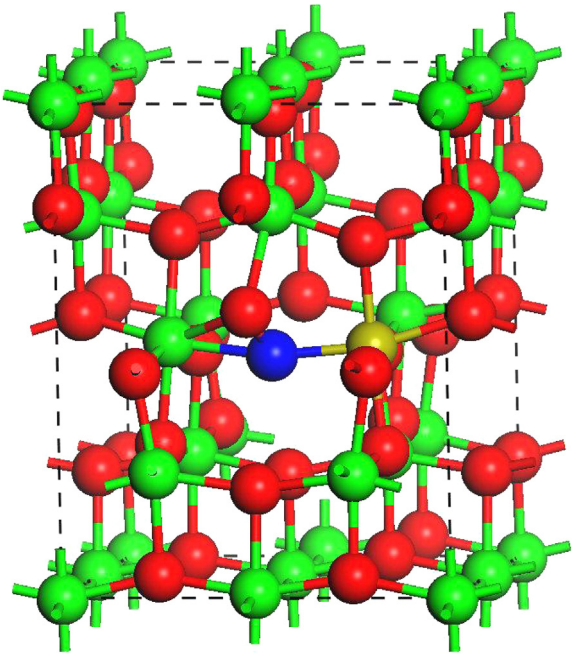

Fig. 9. Optimized structure of Pt_{Ti} and N_{int} co-doped TiO_2 anatase. Green, red, blue and yellowish grey balls represent Ti, O, N, and Pt ions, respectively. (For interpretation of the references to color in this figure legend, the reader is referred to the web version of this article.)

the O sites. This suggests that Pt,N–TiO_2 has different atomic interactions. To further understand this, we also performed the calculations for Pt,N–TiO_2 with a configuration in which Pt occupies the Ti site and N occupies the O site in the lattice ($Pt_{Ti} + N_O$, Case V).

We deduced the electronic density of the states (DOS) for all the above mentioned cases (Fig. 10). In pristine TiO_2, the O 2p states are occupied in the valence band (VB) region and distributed from −5 to 0 eV, while Ti 3d states lie in the conduction band (CB) region. N 2p and Pt 5d states are partially occupied and located in between the VB and CB (Fig. S11) in Pt,N–TiO_2. In N–TiO_2, the occupied N 2p states are located at around 0.5 eV above the top of VB. Similarly, the occupied Pt 5d states lie just above the VB in Pt-TiO_2. Note that the unoccupied states of the N 2p and Pt 5d levels are distributed in the CB region. Because the dopants strongly interact with the bulk system, the hybridized levels are pronounced and extend below the bottom of VB.

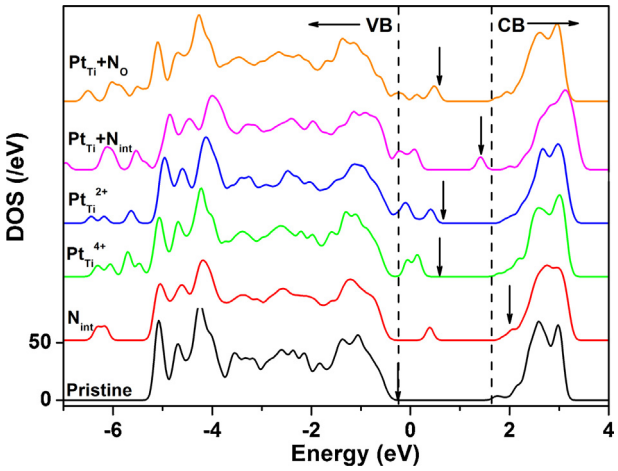

Fig. 10. Total density of states (DOS) of pristine and various doped TiO_2 anatase. Down arrow depicts the Fermi level of respective system. In between VB and CB, the occupied Pt-5d states and the fully or partially occupied N-2p states are pronounced.

It is important to discuss hole transport in TiO_2 nanoparticles based on electronic structure calculations. In general, the photoexcitation of TiO_2 results in the formation of holes lying on top of VB. In the case of N–TiO_2, the N doping induces discrete energy levels lying above the VB of TiO_2 which may restrict hole transportation in the bulk. This level may trap the photogenerated hole and retard the electron–hole recombination. The TDR results reveal that the electron life time is higher with N–TiO_2 in presence of CH_3OH under 355 nm excitation (Fig. 8), which is in good agreement with the electronic structure. In a similar way, the hole transport will be less facile with the Pt^{4+} ($5d^6$) doped case because the Pt 5d levels lie above the VB of TiO_2. On the other hand, when Pt exists as the Pt^{2+} ($5d^8$) ion in TiO_2 (with oxygen vacancy), the occupied Pt 5d states significantly overlap with the states available at the top of VB due to the presence of eight electrons in the 5d orbitals. This could facilitate hole mobility within the bulk of TiO_2. Hence, it is clear that Pt^{2+} ions are responsible for better hole transport in Pt–TiO_2, rather than Pt^{4+} ions. However, in Pt-TiO_2, the presence of both Pt^{2+} and Pt^{4+} may reduce the beneficial role of Pt^{2+} because the energy levels created with Pt^{2+} and Pt^{4+} lie close to each other and may lead to recombination of the photogenerated electron–hole pair. Furthermore, DOS of Pt,N–TiO_2 shows the displacement of the occupied N 2p states based on the doping site of the N atom. In the case of N substituted at the O site, the N 2p states overlap with the Pt 5d states whereas the N 2p states are shifted closer to CB when N is located at the interstitial site. The former case is expected to have high hole mobility than that in the latter configuration. The electronic structure results clearly reveal a difference in the interaction between Pt and N in the co-doped TiO_2 when compared to the case in which they act as individual dopants. This interaction facilitates the charge carrier mobility and reduces the undesired recombination thereby enhancing the photocatalytic activity. Thus, the dopants Pt and N exhibit a synergistic effect in enhancing the photocatalytic activity of TiO_2.

4. Conclusions

The present study shows that the co-doping of Pt ions in N–TiO_2 changes the optical property and enhances the visible light photocatalytic activity with exhibiting synergistic effects. The simultaneous doping of Pt and N enhances visible light absorption compared to bare and N–TiO_2, yet a smaller absorption compared to Pt–TiO_2. Doped Pt ions exist predominantly as Pt^{4+}, while doped N ions exist in the form of $-NO_x$ (cationic doping) in co-doped TiO_2. Among all the samples (bare and doped), Pt,N–TiO_2 is the most active for not only photocatalytic conversion but also photocurrent generation under visible light. Such synergistic effects are attributed to the Pt- and N-induced mid-gap levels in which charge pairs are effectively separated. As revealed in the TDR study, the new mid-gap levels created by co-doping affect the hole trapping while Pt transition ($Pt^{4+} \rightarrow Pt^{2+}$) is dominantly contribute to electron trapping in Pt,N–TiO_2. In contrast to Pt–TiO_2 having both Pt^{2+} and Pt^{4+}, hole trapping (e.g., with Pt^{2+}) in Pt,N–TiO_2 is less probable due to the absence of the Pt^{2+} species and hence hole mobility may increase. The DFT calculations further suggest that the electronic interaction between Pt and N in co-doped TiO_2 facilitates the charge carrier mobility and reduces the charge recombination, resulting in the photocatalytic synergy. Pt and N ions are the common dopants of TiO_2 and the present results will be useful for gaining deeper insights into the roles of dopants in photocatalysis.

Acknowledgments

This work was supported by the Green City Technology Flagship Program funded by KIST (KIST-2012-2E23322), the EPB Center

(No. 2008-0061892), the Global Frontier R&D Program on Center for Multiscale Energy System (2011-0031571), and KCAP (Sogang Univ.) (No. 2012M1A2A2671779) funded by the Korea government (MSIP) through NRF.

Appendix A. Supplementary data

Supplementary material related to this article can be found, in the online version, at http://dx.doi.org/10.1016/j.apcatb.2013.09.034.

References

[1] A. Fujishima, T.N. Rao, D.A. Tryk, J. Photochem. Photobiol., C 1 (2000) 1.
[2] M.R. Hoffmann, S.T. Martin, W. Choi, D.W. Bahnemann, Chem. Rev. 95 (1995) 69.
[3] H. Park, Y. Park, W. Kim, W. Choi, J. Photochem. Photobiol., C 15 (2013) 1.
[4] W. Choi, Catal. Surv. Asia 10 (2006) 16.
[5] H. Park, W. Choi, M.R. Hoffmann, J. Mater. Chem. 18 (2008) 2379.
[6] W. Kim, T. Tachikawa, T. Majima, C. Li, H.J. Kim, W. Choi, Energy Environ. Sci. 3 (2010) 1789.
[7] X. Chen, L. Liu, P.Y. Yu, S.S. Mao, Science 331 (2011) 746.
[8] J. Tao, T. Luttrell, M. Batzill, Nat. Chem. 3 (2011) 296.
[9] W. Choi, A. Termin, M.R. Hoffmann, J. Phys. Chem. 98 (1994) 13669.
[10] S. Kim, S.J. Hwang, W. Choi, J. Phys. Chem. B 109 (2005) 24260.
[11] C. Lettmann, H. Hinrichs, W.F. Maier, Angew. Chem. Int. Ed. 40 (2001) 3160.
[12] R. Asahi, T. Morikawa, T. Ohwaki, K. Aoki, Y. Taga, Science 293 (2001) 269.
[13] S.U.M. Khan, M. Al-Shahry, W.B. Ingler, Science 297 (2002) 2243.
[14] T. Ohno, M. Akiyoshi, T. Umebayashi, T. Mitsui, M. Matsumura, Appl. Catal., A 265 (2004) 115.
[15] T. Tachikawa, M. Fujitsuka, T. Majima, J. Phys. Chem. C 111 (2007) 5259.
[16] V.N. Kuznetsov, N. Serpone, J. Phys. Chem. C 113 (2009) 15110.
[17] J.L. Zhang, Y.M. Wu, M.Y. Xing, S.A.K. Leghari, S. Sajjad, Energy Environ. Sci. 3 (2010) 715.
[18] A.T. Kuvarega, R.W.M. Krause, B.B. Mamba, J. Phys. Chem. C 115 (2011) 22110.
[19] Y. Cong, J. Zhang, F. Chen, M. Anpo, D. He, J. Phys. Chem. C 111 (2007) 10618.
[20] M. Xing, J. Zhang, F. Chen, J. Phys. Chem. C 113 (2009) 12848.
[21] Y. Shen, T. Xiong, T. Li, K. Yang, Appl. Catal., B 83 (2008) 177.
[22] K.Q. Tan, H.R. Zhang, C.F. Xie, H.W. Zheng, Y.Z. Gu, W.F. Zhang, Catal. Commun. 11 (2010) 331.
[23] S. Kim, S.-K. Lee, J. Photochem. Photobiol., A 203 (2009) 145.
[24] H. Kim, W. Choi, Appl. Catal., B 69 (2006) 127.
[25] S. Kim, W. Choi, J. Phys. Chem. B 106 (2002) 13311.
[26] H. Park, W. Choi, J. Phys. Chem. B 108 (2004) 4086.
[27] T. Tachikawa, S. Tojo, K. Kawai, M. Endo, M. Fujitsuka, T. Ohno, K. Nishijima, Z. Miyamoto, T. Majima, J. Phys. Chem. B 108 (2004) 19299.
[28] Y. Park, W. Kim, H. Park, T. Tachikawa, T. Majima, W. Choi, Appl. Catal., B 91 (2009) 355.
[29] W. Kim, T. Tachikawa, T. Majima, W. Choi, J. Phys. Chem. C 113 (2009) 10603.
[30] P.E. Blochl, Phys. Rev. B: Condens. Matter 50 (1994) 17953.
[31] L.H. Huang, C. Sun, Y.L. Liu, Appl. Surf. Sci. 253 (2007) 7029.
[32] P.A. Cox, The Electronic Structure and Chemistry of Solids, Oxford University Press, Oxford, 1987.
[33] Z.S. Jin, Z.S. Chen, Q.L. Li, C.J. Xi, X.H. Zheng, J. Photochem. Photobiol., A 81 (1994) 177.
[34] X.F. Qiu, C. Burda, Chem. Phys. 339 (2007) 1.
[35] S. Livraghi, A. Votta, M.C. Paganini, E. Giamello, Chem. Commun. (2005) 498.
[36] N. Serpone, J. Phys. Chem. B 110 (2006) 24287.
[37] K. Nakamoto, Infrared and Raman Spectra of Inorganic and Coordination Compounds, fifth ed., John Wiley & Sons, New York, 1997.
[38] C. Sedlmair, K. Seshan, A. Jentys, J.A. Lercher, J. Catal. 214 (2003) 308.
[39] G. Yang, Z. Jiang, H. Shi, T. Xiao, Z. Yan, J. Mater. Chem. 20 (2010) 5301.
[40] NIST, NIST X-ray Photoelectron Spectroscopy Database, 2012, ⟨http://srdata.nist.gov/xps⟩.
[41] T. Meites, L. Meites, Anal. Chem. 27 (1955) 1531.
[42] H. Park, J. Lee, W. Choi, Catal. Today 111 (2006) 259.
[43] T. Yoshihara, R. Katoh, A. Furube, Y. Tamaki, M. Murai, K. Hara, S. Murata, H. Arakawa, M. Tachiya, J. Phys. Chem. B 108 (2004) 3817.
[44] S. Tojo, T. Tachikawa, M. Fujitsuka, T. Majima, J. Phys. Chem. C 112 (2008) 14948.